A Population of TIM4$^+$FOLR2$^+$ Macrophages Localized in Tertiary Lymphoid Structures Correlates to an Active Immune Infiltrate Across Several Cancer Types

Mattia Bugatti[1,2], Marco Bergamini[1,3], Francesco Missale[2,4], Matilde Monti[2], Laura Ardighieri[1], Irene Pezzali[2], Sara Picinoli[2], Nicoletta Caronni[5], Yoann Missolo-Koussou[6], Julie Helft[7], Federica Benvenuti[8], and William Vermi[1,2,9]

ABSTRACT

TIM4 has previously been associated with antitumor immunity, yet the pattern of expression and the function of this receptor across human cancer tissues remain poorly explored. Here we combined extensive immunolabeling of human tissues with *in silico* analysis of pan-cancer transcriptomic data sets to explore the clinical significance of TIM4 expression. Our results unveil that TIM4 is expressed on a fraction of cavity macrophages (^{CA}TIM4$^+$MΦ) of carcinoma patients. Moreover, we uncover a high expression of TIM4 on macrophages of the T-cell zone of the carcinoma-associated tertiary lymphoid structures (^{TLS}TIM4$^+$MΦ). *In silico* analysis of a pan-cancer data set revealed a positive correlation between TIM4 expression and markers of B cells, effector CD8$^+$ T cells, and a 12-chemokine signature defining tertiary lymphoid structure. In addition, ^{TLS}TIM4$^+$MΦ were enriched in cancers displaying microsatellite instability and high CD8$^+$ T-cell infiltration, confirming their association with immune-reactive tumors. Both ^{CA}TIM4$^+$MΦ and ^{TLS}TIM4$^+$MΦ express FOLR2, a marker of tissue-resident MΦ. However, ^{CA}TIM4$^+$MΦ had a higher expression of the immunosuppressive molecules TREM2, IL10, and TGFβ as compared with ^{TLS}TIM4$^+$MΦ. By analyzing a scRNA sequence data set of tumor-associated myeloid cells, we identified two TIM4$^+$FOLR2$^+$ clusters coherent with ^{CA}TIM4$^+$MΦ and ^{TLS}TIM4$^+$MΦ. We defined specific gene signatures for each subset and found that the ^{CA}TIM4$^+$ MΦ signature was associated with worse patient survival. In contrast, ^{TLS}TIM4$^+$MΦ gene signature positively correlates with a better prognosis. Together, these data illustrate that TIM4 marks two distinct macrophage populations with distinct phenotypes and tissue localization and that may have opposing roles in tumor immunity.

Introduction

Among T-cell immunoglobulin and mucin domain proteins, TIM4 was initially identified as a ligand for TIM1, the latter representing a potent costimulatory molecule for T cells (1). Subsequently, TIM4 was characterized as a phosphatidylserine (PtdSer) receptor expressed on mouse antigen-presenting cells (2). Its critical role in the engulfment of PtdSer-expressing apoptotic bodies by macrophages (MΦ) and dendritic cells was also confirmed in humans (3). Removal of PtdSer-exposing apoptotic bodies by MΦ is critical for the maintenance of tissue homeostasis and for the prevention of autoimmune responses against intracellular antigens released from dying cells (4). Moreover, removal of PtdSer-expressing antigen-specific T cells in secondary lymphoid organs helps the contraction phase of the immune response, thus leading to peripheral tolerance (5).

TIM4 expression is restricted to antigen-presenting cells in primary and secondary lymphoid tissues (3, 5–7), and experimental mouse models have documented its essential role for the maintenance of the homeostatic state of peritoneal MΦ (8), dermal dendritic cells, and Langerhans cells (9). Other studies found that TIM4 marks long-lived tissue-resident MΦ with self-renewal properties in various tissues (10, 11). In human tissues, TIM4 is restricted to liver Kupffer cells, tangible-body MΦ (TBMΦ), and the splenic white pulp MΦ (3, 7), but data on its expression on human immune cells remain very scant.

The functions of TIM4 in cancer immunity in mouse and in human samples have been explored. TIM4 induces autophagy-mediated degradation of ingested tumor antigens by MΦ and dendritic cells, leading to reduced antigen presentation and antitumor immunity (12). We reported that TIM4 is highly expressed by pulmonary type 1 murine classic dendritic cells (cDC1) and was required for antigen uptake and priming of CD8$^+$ tumor-specific T cells. Accordingly, human *TIM4* transcripts increase the prognostic value of a cDC1 signature and predict responses to PD-1 treatment in lung adenocarcinomas (13). The mouse models of peritoneal carcinomatosis have proposed a protumoral role of TIM4$^+$ MΦ. Omental TIM4$^+$ tissue-resident MΦ support the acquisition of a cancer stem cell–like phenotype and the epithelial–mesenchymal transition of disseminated ovarian cancer cells promoting progression and metastatic spread (10). Moreover, TIM4$^+$ cavity MΦ in ovarian cancer display a high oxidative phosphorylation and mitophagy function mediated by arginase-1 (14). Other work expanded

[1]ASST Spedali Civili di Brescia, Brescia, Italy. [2]Department of Molecular and Translational Medicine, University of Brescia, Brescia, Italy. [3]Department of Clinical and Experimental Science, University of Brescia, Brescia, Italy. [4]Department of Head and Neck Oncology and Surgery Otorhinolaryngology, Antoni Van Leeuwenhoek, Nederlands Kanker Instituut, Amsterdam, The Netherlands. [5]San Raffaele Telethon Institute for Gene Therapy (SR-TIGET), IRCCS San Raffaele Scientific Institute, Milan, Italy. [6]PSL University, Institut Curie Research Center, INSERM U932 and SiRIC, Center for Cancers Immunotherapy, Translational Immunotherapy Team, Paris, France. [7]Université Paris Cité, CNRS, INSERM, Institut Cochin, Phagocytes and Cancer Immunology Laboratory, Paris, France. [8]Cellular Immunology, International Centre for Genetic Engineering and Biotechnology (ICGEB), Trieste, Italy. [9]Department of Pathology and Immunology, Washington University School of Medicine, St. Louis, Missouri.

M. Bugatti, M. Bergamini, and F. Missale equally contributed to this article.

Corresponding Author: William Vermi, University of Brescia, 25123, Brescia, Italy. Phone: 3903-0399-8425; E-mail: william.vermi@unibs.it

Cancer Immunol Res 2022;10:1340–53

doi: 10.1158/2326-6066.CIR-22-0271

our understanding of the protumor role of $TIM4^+$ cavity–resident MΦ by showing their ability to sequester cytotoxic antitumor $PtdSer^+CD8^+$ T cells (15). Together, these findings suggest context-specific, divergent roles of myeloid cells expressing TIM4. The characterization of TIM4 expression on immune cells associated with diverse human tumor types is ill-characterized and represents an important gap in understanding the role of this receptor in cancer.

Here we mapped TIM4 expression on human immune cells infiltrating various human tumors. We detected TIM4 expression in various MΦ populations capturing apoptotic cells and in a population of lymph node MΦ of the interfollicular area. In primary and metastatic cancer tissues, TIM4 expression is absent on conventional tumor-infiltrating MΦ. However, we identified two distinct $TIM4^+$MΦ populations in the tumor microenvironment: those associated with tertiary lymphoid structures (TLS; $^{TLS}TIM4^+$MΦ) and those found in the pleural and peritoneal cavities of carcinoma patients ($^{CA}TIM4^+$MΦ). $^{TLS}TIM4^+$MΦ are mainly "non-phagocytic" and found in the T-cell zone of TLS, whose spatial organization resembles secondary lymphoid organs (16, 17) and are recurrent in immunogenic cancers. TLS represent ectopic secondary lymphoid structures found in cancer and inflamed peripheral tissues (16) and their density predicts good prognosis and response to immunotherapy (18, 19). Single-cell RNA analysis of tumor-infiltrating MΦ in breast tumors by members of our group previously identified a novel MΦ population expressing FOLR2 that localizes in the tumor stroma and within lymphoid aggregates (20). These cells efficiently prime and interact with effector $CD8^+$ T cells. We confirmed that $^{TLS}TIM4^+$MΦ and $^{CA}TIM4^+$MΦ coexpress FOLR2. Accordingly, by exploring a pan-cancer scRNA-seq data set of myeloid cells, we identified two $TIM4^+FOLR2^+$ clusters. One cluster is enriched in *LYVE1*, *SLC40A1*, and *SEPP1* transcripts found in antitumor MΦ, whereas the other is reminiscent of immune-suppressive $TREM2^+$ MΦ. Immunostaining tumor sections revealed the immunosuppressive molecules TREM2 (21, 22), IL10 and TGFβ were highly expressed on $^{CA}TIM4^+$MΦ but not on $^{TLS}TIM4^+$MΦ. All these findings indicate that in addition to protumorigenic body cavity $TIM4^+TREM2^+$MΦ, a novel $TIM4^+$ population is observed in the T-cell area of cancer-associated TLS. Although the exact role of these cells is still undefined, their function within the TLS is likely to be associated with protective immunity.

Materials and Methods

Human tissues

IHC was performed on a set of tissue samples obtained from the archive of the Department of Pathology (ASST Spedali Civili di Brescia, Brescia, Italy). Analyzed tissues included nonlymphoid normal tissues ($n = 42$) and reactive lymphoid normal tissues ($n = 33$). Cancer tissues included samples from tissue microarray ($n = 126$ primary carcinomas; Supplementary Table S1; ref. 23) and whole tissue blocks of primary ($n = 135$) and metastatic ($n = 30$) carcinomas, cell block from pleural effusion ($n = 10$), peritoneal cytological specimen ($n = 10$), pleural biopsies ($n = 5$), and peritoneal biopsies ($n = 10$) from lung and ovarian cancer specimens. The study was approved by the local IRB (WW-IMMUNOCANCERhum, NP-906, NP-1284) and conducted in accordance with the Declaration of Helsinki.

Cell-block preparation

Cytologic specimens from pleural and peritoneal effusion were centrifuged for 10 minutes at 3,000 rpm. A solution of plasma (100 μL, kindly provided by Centro Trasfusionale, ASST Spedali Civili di Brescia, Brescia, Italy) and HemosIL8 RecombiPlasTin 2G (200 μL, Instrumentation Laboratory; cat. no. 0020003050; 1:2) were added to cell pellets, mixed until the formation of a clot, and then placed into a labeled cassette. The specimen was fixed in 10% formalin (Bio-Optica; cat. no. 05-K01004) for 1 hour followed by paraffin inclusion.

IHC and digital image analysis

Four micron-thick tissue sections were obtained from formalin-fixed, paraffin-embedded blocks. For IHC staining, endogenous peroxidase was blocked by incubation with methanol (Honeywell, cat. 603-001-00-X) and hydrogen peroxide (AppliChem; cat. no. 141076,1211) 0.03% for 20 minutes during rehydration. Immunostaining was performed using a set of primary antibodies (Supplementary Table S2) after pretreatment with microwave or waterbath in citrate buffer at pH 6.00 or EDTA buffer at pH 8.00, as indicated in Supplementary Table S2. The reaction was revealed using the Goat-on-rodent-HRP-System (Biocare Medical; cat. no. GHP516H) or Novolink Polymer (Leica Microsystems; cat. no. RE7280-CE) followed by diaminobenzidine (DAB, Dako; cat. no. K3467). Finally, the slides were counterstained with Meyer's Haematoxylin (Bio-Optica; cat. no. 05-M06002).

For double staining, after completing the first immune reaction, the second was visualized using Mach 4 MR-AP (Biocare Medical; cat. no. M4U536L) or Goat-on-rodent AP-System (Biocare Medical; cat. no. GAP514G), followed by Ferangi Blue (Biocare Medical, cat. no. FB813S). Localization of $TIM4^+$ cells within tertiary lymphoid structures was confirmed by double and triple staining combining TIM4 with CD20 and CD3. For triple IHC the third immune reaction was revealed using Mach 4 MR-AP (Biocare Medical), followed by ImmPACT Vector Red Substrate Kit, Alkaline Phosphatase (Vector Laboratories, cat. no. SK-4205).

For double sequential immunostains, the first reaction is deleted after first chromogen destain and stripping. Anti-TIM4 was used for the first immune reaction, revealed using Goat on rodent-HRP-Polymer (Biocare Medical) and developed in 3-amino-9-ethylcarbazole chromogen (AEC), counterstained with hematoxylin and cover-slipped using gelatin. Subsequently, the slides were digitally scanned, using Aperio Scanscope CS (Leica Microsystems). After coverslip removal, AEC was washed out and the slides were eluted using a 2-Mercaptoethanol (Fluka, cat. no. 63689)/SDS (Sigma-Aldrich, cat. no. L3771) solution (20 mL 10% w/v SDS with 12.5 mL 0.5 M Tris-HCl, pH6.8, 67.5 mL distilled water and 0.8 mL 2-ME). Slides were subsequently incubated in this solution in a waterbath preheated at 56°C for 30 minutes. Sections were washed for 1 hour in distilled water. After unmasking in microwave, anti-CD163,was revealed using Novolink Polymer (Leica) and AEC. The subsequent immunostains for anti-FOLR2 and anti-TREM2 was developed analogously, anti-FOLR2 was revealed using AEC and diaminobenzidine, respectively. CD3 was revealed using Mach 4 MR-AP and Ferangi blue as chromogen, and slides were counterstained with hematoxylin, cover-slipped, and digitally scanned. The digital slides were processed using ImageScope. Slides were synchronized and corresponding tissue regions were analyzed.

TLS count was performed in a cohort of 76 human lung adenocarcinomas (LUAD). Tumor-associated TLS were identified as ectopic dense mixed lymphoid aggregates composed of $CD20^+$ B cells and $CD3^+$ T cells located at the periphery of the neoplastic area (invasive margin) or in the surrounding noninvolved lung tissue. TLS count was performed on representative tumor sections containing enough non-involved tumor area, as evaluated on hematoxylin and eosin (H&E)

stained sections and was based on a three-tiered score (0 = absence of TLS; 1 = <5 TLS; 2 = ≥5 TLS). $CD8^+$ T-cell density was performed using Aperio Scanscope on digitalized sections. Stained slides were acquired using the Aperio CS2 digital scanner and ScanScope software (Leica biosystems). The whole tumor area was considered for the analysis, with the exclusion of necrotic areas. Data are expressed as absolute number of $CD8^+$ cells per mm^2. Pearson correlation analysis and one-way ANOVA test with *post hoc* pairwise comparisons (Tukey correction for multiple comparisons) were performed between log_2CD8^+ T-cell density and TLS score.

Data processing of the TCGA data sets and statistical analysis

Raw counts for primary solid tumor samples of nine TCGA projects (TCGA-BLCA, TCGA-BRCA, TCGA-COAD, TCGA-HNSC, TCGA-LUAD, TCGA-LUSC, TCGA-OV, TCGA-SKCM, and TCGA-UCEC) were downloaded from GDC Legacy Archive (hg19) using the TCGA biolinks R/Bioconductor package (n = 3,850 cases). Normalized expression was obtained by upper quartile normalization measured in RSEM. For downstream analysis, the log-RSEM gene expression was considered. Gene expression of TIM4, TREM2, FOLR2, CD163, PAX5, CD247 (CD3) and of 12 chemokines (CCL2, CCL3, CCL4, CCL5, CCL8, CCL18, CCL19, CCL21, CXCL9, CXCL10, CXCL11, and CXCL13) was retrieved. The geometric mean of the 12 chemokines genes was defined as TLS signature (24, 25).

Qualitative variables were described as absolute and relative frequencies; standard descriptive statistics were used for continuous variables, expressing means, standard deviations, medians, and ranges. Correlations between quantitative variables were computed using the Pearson correlation coefficient, a Bonferroni's correction of significance was applied for multiple testing in each analysis.

The main outcome was considered the TIM4 gene expression, considered as dependent variable in the multivariable linear regression models. For achieving a qualitative description of coexpression of PAX5, CD3, and a 12-gene panel of chemokines defining the TLS signature, an exact Barnes–Hut t-distributed stochastic neighbor embedding (tSNE) was computed considering Z-scored immune cells infiltration, with Euclidean distance as similarity measure (26). Survival analysis was performed considering the overall survival (OS) and disease-free survival (DFS) as endpoints, and applying Cox proportional hazards models, stratified for tumor site and stage. Partial effects plots and graphs were rendered through "rms," "ggplot2," and "Rtsne" packages. In all analyses, a two-tailed P value < 0.05 was considered significant, and R (version 4.0.2) was used for statistical analysis and rendering graphs.

RNAscope

To localize IL10- and TGFß-positive cells, tissues were analyzed with RNAscope assay (Advanced Cell Diagnostics, Newark) using RNAscope 2.5 HD Assay-RED kit and Hs-IL10 probe (cat no. 602051) recognizing the nt 122–1,163 of the IL10 mRNA (reference sequence NM_000572.2) and Hs-TGFB1 probe (cat. no. 400881) recognizing the nt 170–1,649 of the TGFB mRNA (reference sequence NM_000660.4). The sections from fixed human tissue blocks were treated following the manufacturer's instructions. Briefly, freshly cut 3-μm sections were deparaffinized in xylene (Bio-Optica, cat. no. 06-1304F) and treated with the peroxidase block solution (ACD, cat. no. 322335) for 10 minutes at room temperature followed by the retrieval solution for 15 minutes at 98°C and by protease plus (ACD, cat. no. 322331) at 40°C for 30 minutes. Control probes included Hs-POLR2a-C2 (cat. no. 310451) and dapB-C2 (cat. no. 310043-C2). The hybridization was performed for 2 hours at 40°C. The signal was revealed using RNAscope 2.5 HD Detection Reagent and FAST RED. Combined RNAscope and IHC for TIM4 were used to identify the cellular source of IL10 and TGFß. To this end, IL10 and TGFß detection by RNAscope was combined with immunoreaction visualized using Goat-on-Rodent AP-Polymer followed by Ferangi Blue (Biocare Medical).

Processing of published data set

We downloaded the raw data sets and selected myeloid cells data set (using the article annotation with the mention "Myeloid" in the cell type metadata, 37,334 cells) of Qian and colleagues (36) from a web server (http://blueprint.lambrechtslab.org). Cells were merged using canonical correlation analysis and mutual nearest neighbors, and we selected the 5,000 most variable genes (following the Seurat 3 pipeline). We next performed Louvain graph-based clustering. At resolution 1.2, we obtained 37 clusters. Cluster 25 was expressing TIMD4. We did a subset of this cluster 25 to understand its heterogeneity. We discovered 4 subclusters using the pipeline previously describe. The differential analysis was performed using the Seurat function "FindMarkers" with logistic regression test, adding the tumor tissue type as a variable to correct. The parameter "min.pct" was set at 0.10, which means a gene has to be expressed in at least 10% of cells of a cluster to be considered in the differential analysis. For the visualization (violin and feature plots), we used adaptively thresholded low-rank approximation (ALRA) to improve the plot. ALRA is a pipeline to reduce dropout in a single-cell matrix. With ALRA our matrix went from 4.73% to 11.62% nonzero values. The k parameter calculated by the function "RunALRA" was 19.

To select macrophage-specific transcripts from C0 and C2 clusters, we downloaded the data set of Azizi and colleagues (GSE114725; ref. 27). We used the classic pipeline for single-cell analysis of Seurat V3 (without integration correction) from the raw count matrix (supplementary file GSE114725_rna_raw.csv.gz). We next perform Louvain graph-based clustering. Atresolution 0.9, we obtained 39 clusters: 14 clusters of T cells, 6 clusters of B cells, 5 clusters of NK cells, 1 cluster of pDCs, DC1, DC2, $CD16^+$ monocytes, $CD14^+$ monocytes, neutrophils or mast cells, 3 clusters of macrophages, and 4 clusters of contaminating cells. We merged clusters of the same immune cell types.

Data availability statement

The data generated in this study are available within the article and its supplementary data files. Expression profile data analyzed in this study were obtained from Gene-Expression Omnibus at GSE114725 and for data of TCGA, from GDC Legacy Archive (hg19) using TCGA biolinks R/Bioconductor package, considering the following projects: TCGA-BLCA, TCGA-BRCA, TCGA-COAD, TCGA-HNSC, TCGA-LUAD, TCGA-LUSC, TCGA-OV, TCGA-SKCM, and TCGA-UCEC. Single-cell expression profiles of myeloid cells of Qian and colleagues (36) were downloaded from a web server (http://blueprint.lambrechtslab.org).

Results

TIM4 expression identifies distinct populations of human MΦ

TIM4 expression has been reported in TBMΦ and in cells of the interfollicular area in human tonsils and spleen (3, 7). We extended the analysis of TIM4 expression on an institutional retrospective cohort including reactive lymphoid tissues and nonlymphoid normal tissues. In lymphoid tissues (n = 34), TIM4 expression was confirmed on TBMΦ of reactive tonsils (n = 7) and lymph nodes (n = 16), in sinus

MΦ and cells of the interfollicular area (**Fig. 1A–C**). In tonsils, we could also detect TIM4 reactivity in a minor fraction of 6-sulfo LacNAc$^+$ (slan$^+$) cells, an MΦ population endowed with a high phagocytic capacity (**Fig. 1D**; ref. 23). As previously shown (3, 7), TIM4 reactivity was also detected in spleen MΦ ($n = 6$) that can be divided, based on their location and phenotype, into TIM4$^+$ marginal zone MΦ and TIM4$^+$MΦ in the periarteriolar lymphoid sheaths (**Fig. 1E** and **F**). TIM4$^+$MΦ were also detected in the thymus cortex ($n = 2$) and in the bone marrow ($n = 3$; **Fig. 1G** and **H**). Finally, TIM4 stains TBMΦ and a subset of cells localized in the T-cell area of intestinal Peyer's patches (**Fig. 1I**). Given that TIM4$^+$cells in the nodal interfollicular areas (IF-TIM4$^+$) had not been previously characterized, we set to define this population by double staining with MΦ markers. Indeed, TIM4$^+$interfollicular cells coexpress a large set of MΦ markers (Supplementary Fig. S1). We extended our analysis to dermatopathic lymphadenitis (ref. 28; $n = 4$) and found a population of TIM4$^+$MΦ in T-cell nodules of the paracortex, intermingled with CD3$^+$ T cells (Supplementary Fig. S2). TIM4$^+$TBMΦ, slan$^+$ cells, and thymic and bone marrow MΦ contained visible apoptotic bodies in their cytoplasm, as confirmed by costain for active caspase-3 (Supplementary Fig. S2), whereas TIM4$^+$MΦ in the interfollicular area and in T-cell nodules of dermatopathic lymphadenitis were devoid of intracellular apoptotic bodies (Supplementary Fig. S2). In nonlymphoid tissues ($n = 36$), TIM4 expression was restricted to liver Kupffer cells ($n = 4$) and to a minor fraction of placental Hofbauer MΦ ($n = 4$; Supplementary Fig. S3). Unlike the mouse system (9), skin Langerhans cells ($n = 4$) were TIM4 negative (Supplementary Fig. S3).

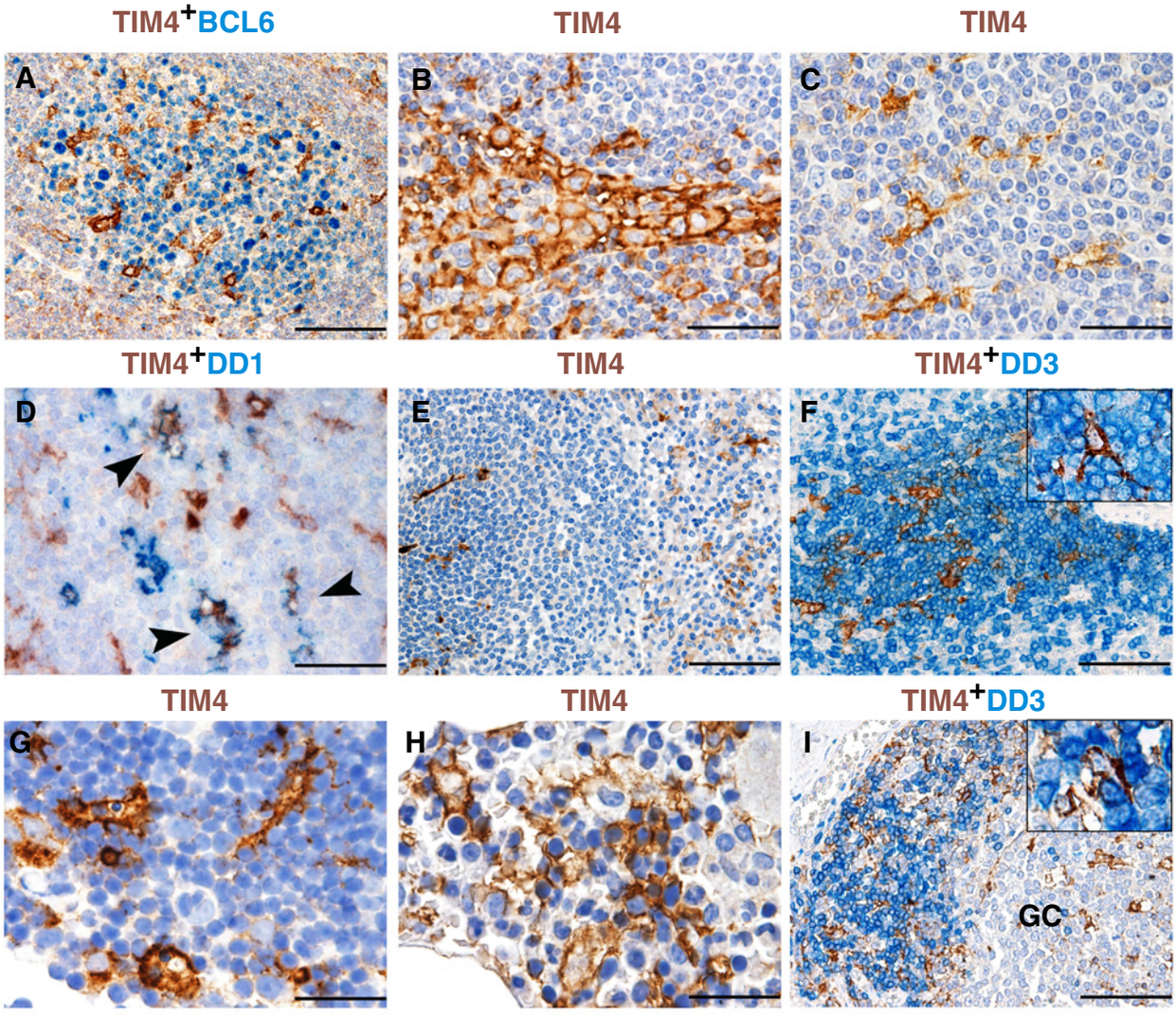

Figure 1.

TIM4 expression in human lymphoid tissues. Sections are from human reactive lymph nodes (**A–C**), tonsil (**D**), spleen (**E** and **F**), thymus (**G**) and bone marrow (**H**), and small intestine (**I**) and stained as labeled. In lymph nodes, TIM4 reactivity is detected in TBMs (**A**), sinus macrophages (**B**), and cells of the interfollicular area (**C**). In tonsils, TIM4 is expressed in a minor fraction of slan+ cells (**D**). TIM4 reactivity is also detected in splenic marginal zone macrophages (**E**) and macrophages of the periarteriolar lymphoid sheaths (**F**). TIM4$^+$ macrophages are detected in the thymus cortex (**G**) and the bone marrow erythroid niches (**H**). In Peyer patches, TIM4 stains TBM and a subset of TIM4$^+$ macrophages localized in the T-cell area (**I**). Magnification: 100× (**A, E, F, I**), scale bar 200 μm; 400× (**B, C, D, G, H**), scale bar 50 μm.

Together, this analysis suggests that besides the already described class of highly phagocytic MΦ, TIM4 is expressed by a second group of nonphagocytic MΦ localized in the T-cell zone of various compartments.

TIM4 marks MΦ in the T-cell zone of carcinoma-associated tertiary lymphoid structures

Emerging findings indicate a complex phenotypic and genetic heterogeneity of tumor-associated MΦ (29–31); however, TIM4 expression on MΦ is poorly characterized in human cancers. Based on our findings on the role of mouse TIM4 in modulating the antitumor T-cell response in carcinomas (13), we further explored TIM4 expression in a set of primary carcinomas using tissue microarray ($n = 126$; ref. 23). No reactivity could be detected in the tumor areas, thus excluding TIM4 expression on conventional tumor-infiltrating MΦ (Supplementary Fig. S4). However, TIM4 expression has been unequivocally detected in cancer tissues based on scRNA sequencing experiments (20). We thus extended our analysis on whole tumor sections, including the peritumoral area, of a cohort of human cancers ($n = 135$) including non–small cell lung cancers ($n = 37$), melanomas ($n = 13$), cutaneous squamous cell carcinomas ($n = 6$), cutaneous sebaceous carcinoma ($n = 1$), colorectal carcinomas ($n = 30$), endometrial carcinomas ($n = 30$), luminal breast carcinomas ($n = 5$), squamous cell carcinomas of the larynx ($n = 8$), and gastric cancers ($n = 5$). The analysis confirms the lack of TIM4 expression on conventional $CD163^+TREM2^+M\Phi$ infiltrating the tumor bed, as observed by immunostaining of sections from a pan-cancer tissue microarray (**Fig. 2A–F**). However, we could detect TIM4 expression in TLS surrounding the tumor area in primary and metastatic carcinomas (**Fig. 2G** and **H**; Supplementary Fig. S5). Immature TLS are composed of small aggregates of T cells, whereas fully mature TLS contain a B-cell area with germinal centers surrounded by a distinct T-cell zone. In addition to TBMΦ, TIM4 marks MΦ in immature TLS (Supplementary Fig. S5) and in the T-cell zone of mature TLS (from here referred to as $^{TLS}TIM4^+$; **Fig. 2I** and **J**). A large fraction (98.64%) of $^{TLS}TIM4^+$ interacted with at least one surrounding T cell. Moreover, TLS-containing $TIM4^+$ cells frequently surrounded $CD34^+$ vessels (Supplementary Fig. S5). Based on double and sequential stains, we could confirm that $^{TLS}TIM4^+$ cells in primary carcinomas express a large set of MΦ markers including MAFB, CD11c, C1q, APOE, CD163L1, CD14, CD163, CD16, CSF1R, PG-M1, and HLA-DR; heterogeneous expression was also found for MS4a4a (**Fig. 3A–L**), an MΦ marker essential for dectin-1–dependent activation of NK cell–mediated resistance to metastasis (32). Finally, based on double stains for active caspase-3, we observed that $^{TLS}TIM4^+$ cells in primary carcinomas more rarely contain apoptotic cells/bodies compared with other $TIM4^+M\Phi$ (**Fig. 3M** and **N**).

All these findings are in keeping with the existence of a specific $TIM4^+M\Phi$ population (from here referred to as $^{TLS}TIM4^+M\Phi$) found in the T-zone of TLS, mostly interacting with T cells.

High TIM4 expression identifies immune-infiltrated immunogenic cancers enriched in TLS

Our microscopy findings suggest that $^{TLS}TIM4^+M\Phi$ are restricted to the group of TLS-containing carcinomas. This subgroup is particularly enriched in effector T cells and characterized by a better outcome (16). By analyzing transcriptional profiles of a large set ($n = 3{,}850$) of human carcinomas from different primary sites (9 TCGA projects), we found that TIM4 expression strongly and positively correlates with the expression of a set of genes associated with infiltration of B cells (PAX5; $R = 0.38$, $P < 0.001$; **Fig. 4A**) and T cells (CD3; $R = 0.46$, $P < 0.001$; **Fig. 4B**). Moreover, TIM4 expression correlates with a TLS signature composed of 12 TLS-related genes previously defined and validated (ref. 25; $R = 0.46$, $P < 0.001$; **Fig. 4C**). As visualized by tSNE, a group of cases across various cancer types (LUAD, LUSC, HNSC, and BRCA) resulted particularly enriched by TIM4, PAX5, CD3 transcripts, and the 12 TLS-related genes (**Fig. 4D–J**).

Immunogenic cancers are also defined by a high density of $CD8^+$ T cells (33, 34). We analyzed an institutional retrospective cohort of human LUAD and LUSC ($n = 74$) and found that a significant fraction contained TLS ($n = 53$; 71.6%). TLS regularly comprises $^{TLS}TIM4^+M\Phi$ and their density directly correlates with the density of $CD8^+$ T cells, as measured by digital microscopy (Supplementary Fig. S6A and S6B). This finding was also confirmed on the TCGA data sets both in LUSC ($R = 0.55$, $P < 0.001$) and LUAD ($R = 0.34$, $P < 0.001$), showing direct and positive correlation between TIM4 and CD8 transcripts.

To reinforce the notion that $TIM4^+$ cells may be enriched in immunoreactive tumors carrying abundant TLS we turned to analyze microsatellite unstable (MSI^+) colorectal carcinomas (COAD), well-established examples of immune-infiltrated tumors (35). We directly correlated the occurrence of $^{TLS}TIM4^+M\Phi$ in COAD with associated DNA mismatch-repair defects (MLH-1 and PMS2) by IHC ($n = 30$; Supplementary Fig. S6C). $^{TLS}TIM4^+M\Phi$ were detected in most of the COAD cases ($n = 26/30$; 86%); however, its expression was restricted to TLS, resulting in largely negative conventional tumor-infiltrating MΦ. Molecular classifications have identified four consensus molecular subgroups of COAD according to their clinical, molecular, and immune features. Of note, CMS1 (containing MSI cases) and CMS4 are immune-infiltrated and highly enriched in TLS signature (Supplementary Fig. S6D), the latter being highly correlated with TIM4 expression (Supplementary Fig. S6E).

These findings indicate that $^{TLS}TIM4^+M\Phi$ are enriched in immune-infiltrated highly immunogenic cancers where they remain confined to the T-cell zone of TLS.

$^{TLS}TIM4^+M\Phi$ are transcriptionally distinct from tumor-infiltrating MΦ

Tumor-infiltrating MΦ populations in human cancers show distinct phenotypes and localization, as revealed by the expression of TREM2 and FOLR2. $FOLR2^+M\Phi$ are spatially segregated from $TREM2^+M\Phi$ across human cancers (21), with a mutually exclusive expression (20). Specifically, $TREM2^+M\Phi$ infiltrated the tumor nest, and its expression inversely correlated with patient survival in triple-negative breast cancer and colorectal cancer (21). By contrast, $FOLR2^+M\Phi$ remain in the peritumoral stroma (20). Of note, $FOLR2^+M\Phi$ could also be detected within TLS, and TIM4 transcript is part of the signature defining $FOLR2^+M\Phi$ (20). To further extend this finding, we analyzed a set of primary carcinomas (TCGA; $n = 3{,}850$; BLCA = bladder cancer; BRCA = breast cancer; COAD = colorectal cancer; HNSC = Head&Neck squamous cell carcinomas; LUAD = lung adenocarcinomas; LUSC = lung squamous cell carcinomas; OV = ovarian carcinomas; SKCM = skin cutaneous melanomas; UCEC = uterine corpus endometrial carcinoma). A multivariable linear regression model was fitted including covariates TIM4, TREM2, FOLR2, the tumor site, the stage, the TLS signature, PAX5, and CD3. The significantly direct correlation between PAX5, CD3, TLS, FOLR2 signature, and TIM4 expression was confirmed (**Fig. 5A–D**, $P < 0.001$), whereas a lack of association was found with TREM2 expression (**Fig. 5E**). Accordingly, by dimensionality reduction, the cluster $PAX5^{High}CD3^{High}TLS^{High}$ was enriched of TIM4 and

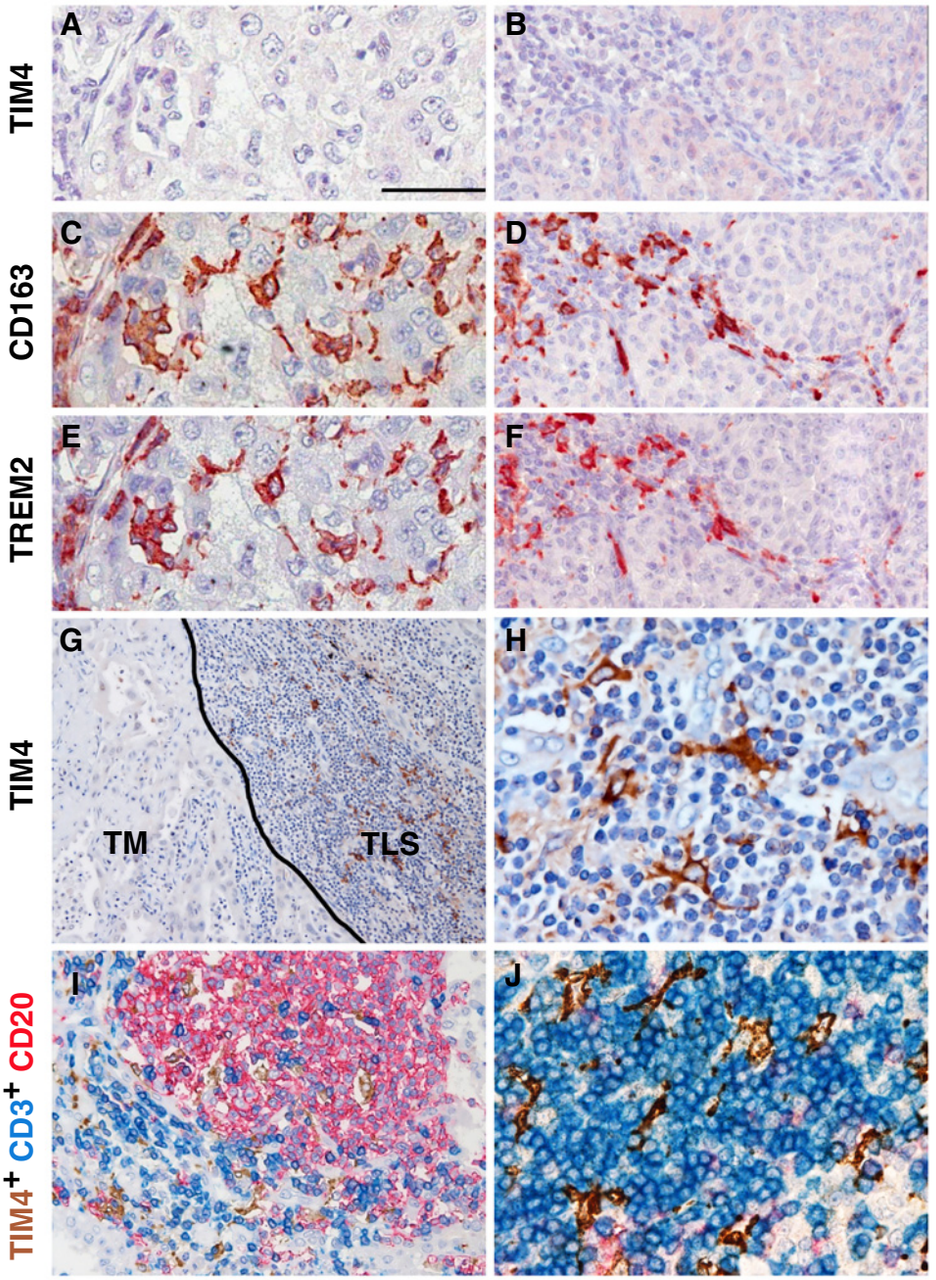

Figure 2.

$TIM4^+$ macrophages in human cancers. Sections are from human high-grade serous ovarian carcinoma (**A–F**), lung adenocarcinoma (**G, H**), and squamous cell carcinoma of the larynx (**I, J**) and stained as labeled. TIM4 expression is absent on conventional $CD163^+$ $TREM2^+$ macrophages (**A–F**), as illustrated by sequential immunostain (performed on the same tissue section), but is detected in mature tertiary lymphoid structures surrounding the tumor area (**G**, low power view; **H**, high power view). Triple stain for CD20, CD3, and TIM4 highlights the localization of $TIM4^+$ cells in the B- and T-cell zone of the TLS (**I**) and their interaction with T cells (**J**, high power view). Magnification: 400× (**A–F, H, J**) scale bar 50 μm; 100× (**G**), scale bar 200 μm; 200× (**I**), scale bar 100 μm.

FOLR2 but not of TREM2 (**Fig. 5F–I**). These observations confirm a direct positive correlation in cancer tissues between FOLR2 and TIM4 expression with the local adaptive immune response and TLS formation.

To gain further insight into the transcriptional profile of $^{TLS}TIM4^+MF$, we explored a pan-cancer scRNA-seq data set (36) comprising ovarian, breast, lung, and colorectal cancers. We merged 37,334 myeloid cells from all cancer types. Louvain graph-based clustering at the resolution 1.2 identified 37 clusters of mononuclear phagocytes (**Fig. 6A**). We identified a discrete cluster (C25) enriched in *TIMD4* expression and macrophage transcripts (*CD163, C1QA, APOE, MAF*; ref. 37; **Fig. 6B** and **C**; Supplementary Table S3). We next investigated the heterogeneity of $TIMD4^+$ C25. To this end, we performed a new Louvain graph clustering of C25 and found 4 transcriptionally distinct subclusters (C0 to C4) at resolution 0.3 (**Fig. 6D**). The distinct subclusters expressed variable amounts of *FOLR2, TIMD4*, and *TREM2* (**Fig. 6E**). C0 and C2 expressed *FOLR2* and *TIMD4* more highly, as compared with C1 and C3 (**Fig. 6E**). This result suggests that C0 and C2 could represent $^{TLS}TIM4^+M\Phi$ and $^{CA}TIM4^+M\Phi$. We found 50 differentially expressed genes between C0 and C2 (Supplementary Table S4). Among those genes, C2, with the highest expression of *FOLR2*, was enriched in *LYVE1*, *SLC40A1*, and *SEPP1* (**Fig. 6E**; Supplementary Table S5). We have previously shown that these transcripts are enriched in mammary gland-resident $FOLR2^+$ macrophages and predict good prognosis in a subgroup of breast cancer patients (20). C0 was enriched in genes reminiscent of

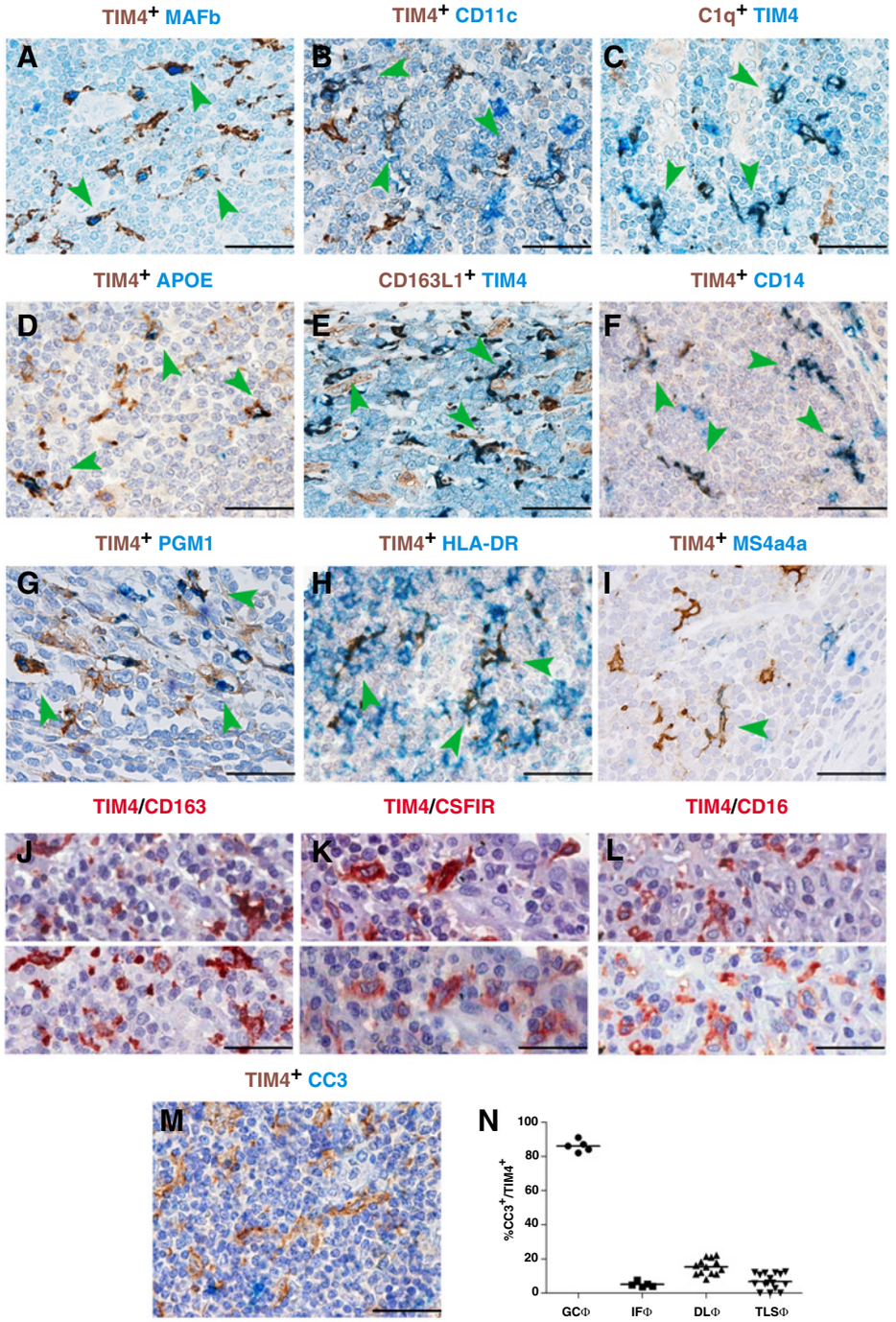

Figure 3.

Phenotype of ^{TLS}TIM4^{+} macrophages in human cancer. Sections are from HNSCC (**A–M**) and stained as labeled. Double stain showing reactivity of ^{TLS}TIM4^{+} macrophages to a large set of macrophage markers including MAFB (**A**), CD11c (**B**), C1q (**C**), APOE (**D**), CD163L1 (**E**), CD14 (**F**), PG-M1 (**G**), and HLA-DR (**H**); heterogeneous expression was found for MS4a4a (**I**). Sequential stains for TIM4 coupled with CD163 (**J**), CSF1R (**K**), and CD16 (**L**) showing coexpression of these markers in ^{TLS}TIM4^{+} macrophages. By double stain for TIM4 and cleaved caspase-3 (CC3) ^{TLS}TIM4^{+} macrophages are rarely engulfed by apoptotic cells/bodies (**M, N**). Magnification 400× (**A–M**), scale bar 50 micron; GC = germinal center; IF = interfollicular area; DL = dermatopathic lymphadenitis; TLS = tertiary lymphoid structures.

TREM2^{+} macrophages including *TREM2*, *FCN1*, and *PLAUR* (**Fig. 6E**; Supplementary Table S4; refs. 20, 21). We, therefore, concluded that *TIMD4*$^{+}$MΦ encompass two types of MΦ that might have a distinct function in the tumor microenvironment. *TIMD4*$^{+}$ MΦ expressing *FOLR2* highly and *TREM2* lowly (C2) could be ^{TLS}TIM4^{+}MΦ and could support antitumor responses as previously described for mammary gland–resident FOLR2^{+} macrophages (20). *TIMD4*$^{+}$ MΦ expressing *TREM2* highly (C0) could be ^{CA}TIM4^{+} MΦ with protumorigenic functions, as previously seen for TREM2^{+} macrophages (21, 38) or TIM4^{+} cavity and omentum resident macrophages (10, 15). We integrated the information derived from a previously defined expression matrix (ref. 20; Supplementary Fig. S7), by selecting among macrophage-restricted transcripts of the C0 and C2 clusters to be included in the definition of ^{TLS}TIM4^{+}MΦ (average scaled expression of TIMD4, FOLR2, SEPP1, SLC40A1, PMP22, MAMDC2, and NEURL2) and ^{CA}TIM4^{+} MΦ (average scaled expression of TIMD4, TREM2, PLAUR, FN1, FCN1, and OLR1) signatures. By exploring the TCGA data set with a pan-cancer analysis,

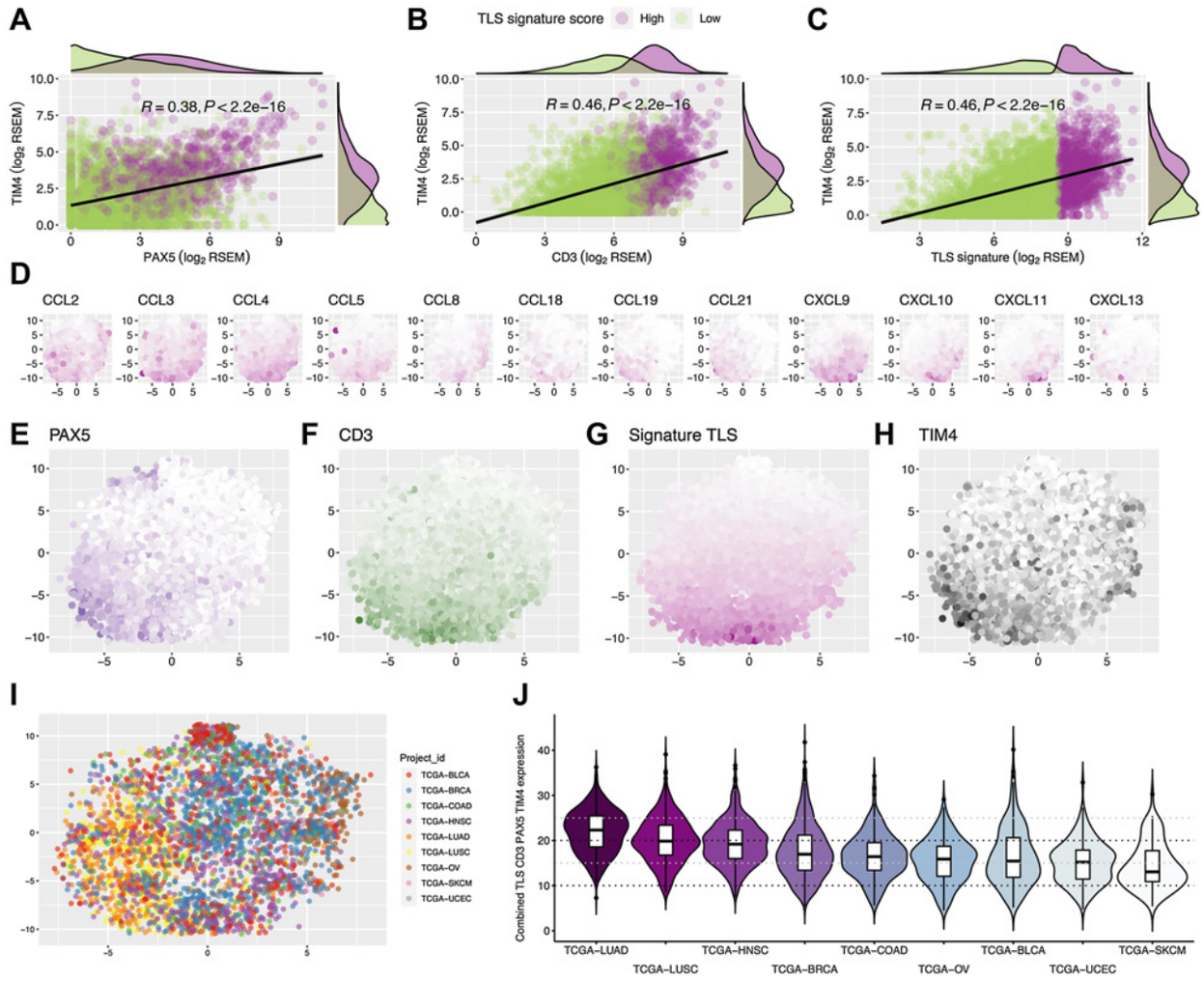

Figure 4.

TIM4 correlation with high lymphoid infiltration and TLS signature. Scatter plots showing the correlations between PAX5 (**A**), CD3 (**B**), TLS signature (**C**), and the TIM4 expression by Pearson test linear regression lines; colored marginal density plots highlight the TLS^{Low} and TLS^{High} groups applying as cutoff points the third quartile of TLS signature score distribution. tSNE plots devised by dimensionality reduction according to the expression of the 12 genes defining the TLS signature (**D**), PAX5 (**E**), and CD3 (**F**); the overall TLS signature score (**G**), the TIM4 expression (**H**), and tumor sites (**I**) are shown. Violin plots and box plots showing the sum of PAX5, CD3, TLS signature, and TIM4 among different tumor sites, in descending order according to the median values (**J**). Forest plots of two multivariable Cox models (both stratified for stage and TCGA project) of DFS and OS exploring in the selected data sets of the TCGA the clinical significance of the $^{CA}TIM4^{+}$ MΦ signature (average scaled expression of TIMD4, TREM2, PLAUR, FN1, FCN1, and OLR1) and of the $^{TLS}TIM4^{+}$MΦ one (average scaled expression of TIMD4, FOLR2, SEPP1, SLC40A1, PMP22, MAMDC2, and NEURL2); HR with 95% CI is shown. BLCA, bladder cancer; BRCA, breast cancer; COAD, colorectal cancer; HNSC, Head&Neck squamous cell carcinomas; LUAD, lung adenocarcinomas; LUSC, lung squamous cell carcinomas; OV, ovarian carcinomas; SKCM, skin cutaneous melanomas; UCEC, uterine corpus endometrial carcinoma.

we found that a higher expression of the $^{CA}TIM4^{+}$ MΦ signature is associated with a significant worse DFS ($P = 0.0093$) and OS ($P = 0.005$), whereas a higher expression of the $^{TLS}TIM4^{+}$MΦ signature predicts a significantly better DFS ($P = 0.0096$; **Fig. 6F** and **G**).

Cavitary $TIM4^{+}$MΦ in pleural and peritoneal carcinoma localizations express immunosuppressive molecules

Studies on lung and ovarian cancer indicate that TIM4-expressing MΦ are found in pleural and peritoneal cavities as well as in the infiltrated omentum (10, 14, 15). Their occurrence has been associated with metastatic spread and worse outcome (10, 15), due to their capability to sequester neighboring T cells. By staining cell-block sections, cavitary $TIM4^{+}$MΦ were observed in fluid from noncancer patients ($n = 5$) as a minor fraction of $CD163^{+}$MΦ (**Fig. 7A**). In pleural ($n = 10$) and peritoneal effusion ($n = 10$) of patients with primary lung and ovarian carcinomas, we could confirm the existence of a cavity $TIM4^{+}$MΦ subpopulation (from here referred as $^{CA}TIM4^{+}$MΦ) in all samples ($n = 10/10$; **Fig. 7A**), showing a significantly increased percentage compared with non-neoplastic fluid ($P = 0.0125$; **Fig. 7A**). We subsequently analyzed pleural and peritoneal biopsies from the same patient group and found that similar to other carcinoma sites, they also contained $^{TLS}TIM4^{+}$MΦ (**Fig. 7A**). These microscopy findings identify two distinct $TIM4^{+}$ MΦ populations in patients with pleural and

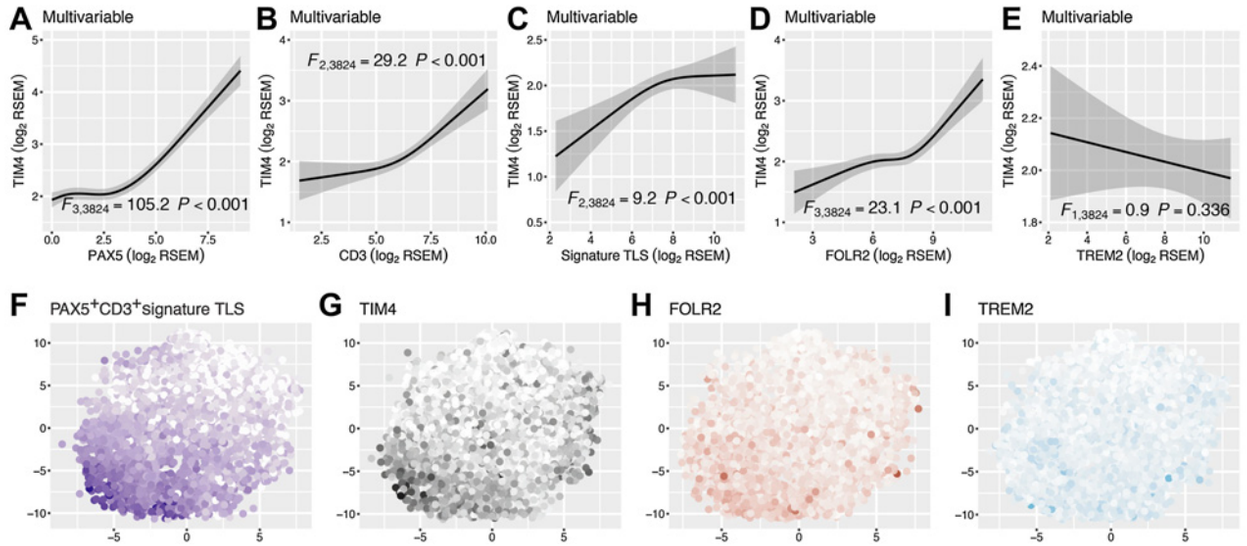

Figure 5.

Coordinated expression of TIM4 and FOLR2 but not TREM2 in immune-infiltrated carcinomas. Partial effects plots derived from the multivariable linear regression model (multicancer TCGA data set; $n = 3{,}850$) for the prediction of TIM4 expression, showing its association with PAX5, CD3, TLS signature score, and FOLR2, but not with TREM2 expression (**A–E**). tSNE plots highlighting the PAX5^{High}CD3^{High}TLS^{High} cluster (**F**) enriched in TIM4 (**G**) and FOLR2 (**H**) but not associated with the TREM2 expression (**I**).

peritoneal effusions, including ^{CA}TIM4^{+}MΦ and ^{TLS}TIM4^{+}MΦ. We subsequently compared these two populations by phenotypes (**Fig. 7B**). By using multiple sequential stains, we found that ^{CA}TIM4^{+}MΦ express regularly TREM2 (86.39%) and coexpress FOLR2, whereas ^{TLS}TIM4^{+}MΦ expressed FOLR2 but lack TREM2 (**Fig. 7B**; Supplementary Fig. S8).

Moreover, a major fraction of ^{TLS}TIM4^{+}FOLR2^{+}TREM2^{-}MΦ (98.64%) interacted with CD3^{+} T cells (**Fig. 7C**). A similar phenotype (TIM4^{+}FOLR2^{+}TREM2^{-}) was confirmed in MΦ of the interfollicular area in reactive lymphoid organs (Supplementary Fig. S8).

These findings indicate the existence of two TIM4^{+}MΦ populations showing phenotypic diversity and distinct localization. TREM2 expression by ^{CA}TIM4^{+}MΦ might likely account for their detrimental prognostic significance (10, 15). To further extend our analysis at the functional level, we tested the expression of IL10 and TGFβ by TIM4^{+}MΦ in carcinoma-associated TLS ($n = 7$) and in pleural/peritoneal effusions ($n = 5$). Of relevance, only ^{CA}TIM4^{+}MΦ showed a detectable and abundant IL10 and TGFβ mRNA signal, whereas ^{TLS}TIM4^{+}MΦ resulted largely negative (**Fig. 7D**), as proved by combining TIM4 immunostaining and RNAscope *in situ* hybridization. Based on these findings, we quantified CD3^{+}Foxp3^{+} regulatory T cells (Treg) in cell blocks sections of pleural and peritoneal fluids and found an increased percentage of Treg in neoplastic cases compared with reactive conditions (Supplementary Fig. S9).

These findings confirm the existence of distinct TIM4^{+} populations with diverse subtissular localization that may be associated with different functions.

Discussion

TIM4 expression on human immune cells has been poorly investigated. By microscopic mapping, this study analyzed the cellular localization of TIM4 on human tissues. As previously reported (3, 7), we confirm that TIM4 is predominantly expressed on MΦ in secondary lymphoid organs. TIM4^{+}MΦ are also detected in the thymus and bone marrow. Among nonlymphoid organs, only liver Kupffer cells and a fraction of placenta Hofbauer cells were positive for TIM4. The most relevant and novel finding of this study was found in the analysis of cancer tissues. Specifically, TIM4 is lacking in conventional carcinoma-infiltrating MΦ but is expressed in specific MΦ of the T-cell zone in the tertiary lymphoid structures (referred to as ^{TLS}TIM4^{+}MΦ) and in a fraction of cavity MΦ (referred to as ^{CA}TIM4^{+}MΦ). The existence of ^{TLS}TIM4^{+}MΦ was never reported, whereas ^{CA}TIM4^{+}MΦ has been previously described (10). Based on *in silico* and IHC data, we envisage a protective role of ^{TLS}TIM4^{+}MΦ by promoting adaptive T-cell immunity, whereas ^{CA}TIM4^{+}MΦ might represent a protumor immune cell population based on their expression of TREM2.

As a novel finding on lymphoid tissues, this study uncovers TIM4 expression on cells of the interfollicular area. TIM4^{+} interfollicular cells coexpress MΦ markers, thus corresponding to a fraction of nodal MΦ. TIM4 reactivity was also observed in dermatopathic lymphadenitis, particularly in MΦ intermingled with CD3^{+} T cells in T-cell nodules of the paracortex. As has been shown (39), TIM4 plays a relevant role in the clearance of apoptotic B cells in germinal centers by TBMΦ (2). We could document colocalization of TIM4 and active caspase-3^{+} apoptotic cells/bodies in TBMΦ. A similar finding was observed on thymic and bone marrow TIM4^{+}MΦ as well as on tonsils slan^{+} cells, an MΦ population with a high phagocytic capacity (23). Thymic TIM4^{+}MΦ regulate T cell–positive selection (40, 41), whereas bone marrow TIM4^{+}MΦ engulf PtdSer-exposing nuclei expelled from erythroid precursor cells during red blood cells maturation (42) and are thought to supply the erythroblasts with iron and growth factors (43). As documented in our previous study, slan^{+} MΦ containing neoplastic B cells are detected in diffuse large B-cell lymphoma (44). At variance with TIM4^{+}MΦ clearing of apoptotic cells, we found TIM4^{+}MΦ from the interfollicular area, as well as ^{TLS}TIM4^{+}MΦ, rarely contain apoptotic bodies. This finding suggests

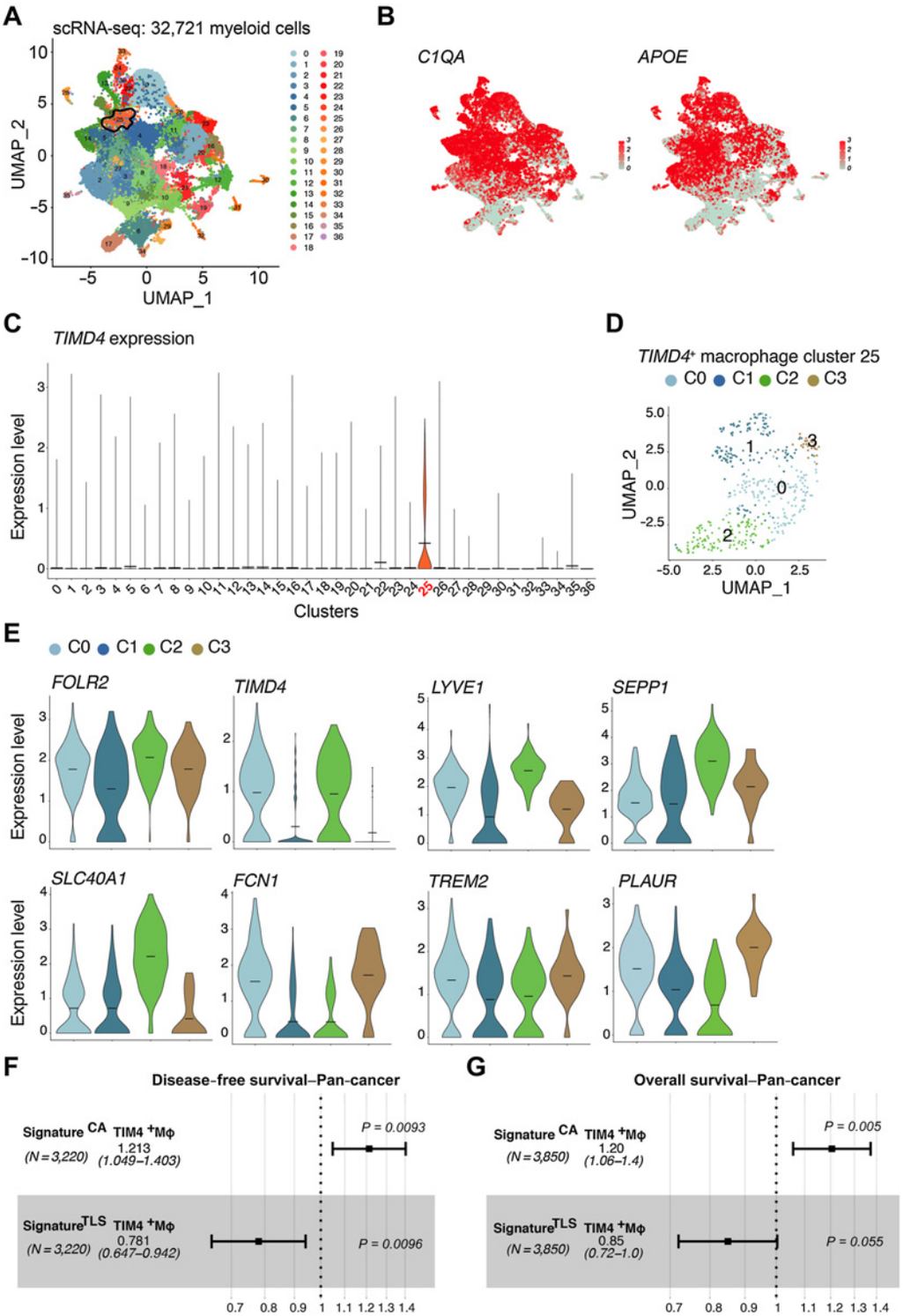

Figure 6.

scRNA-seq analysis of myeloid cells across cancer types. Dimensionality reduction of scRNA-seq data merged from lung, colorectal, ovarian, and breast tumors was performed using a Louvain graph-based clustering identifying 37 clusters (middle). Each dot represents an individual cell ($n = 37{,}334$; **A**). Dimensionality reduction of scRNA-seq for C1QA and APOE (**B**). Violin plots illustrating expression distributions among the 37 clusters of TIMD4 (right; **C**). UMAP visualization of TIMD4^{+} macrophages (cluster 25) at a 0.3 resolution (**D**). Expression distributions of *FOLR2*, *TIMD4, LYVE1, SEPP1, SLC40A1, FCN1, TREM2*, and *PLAUR* across macrophage of C25 (**E**).

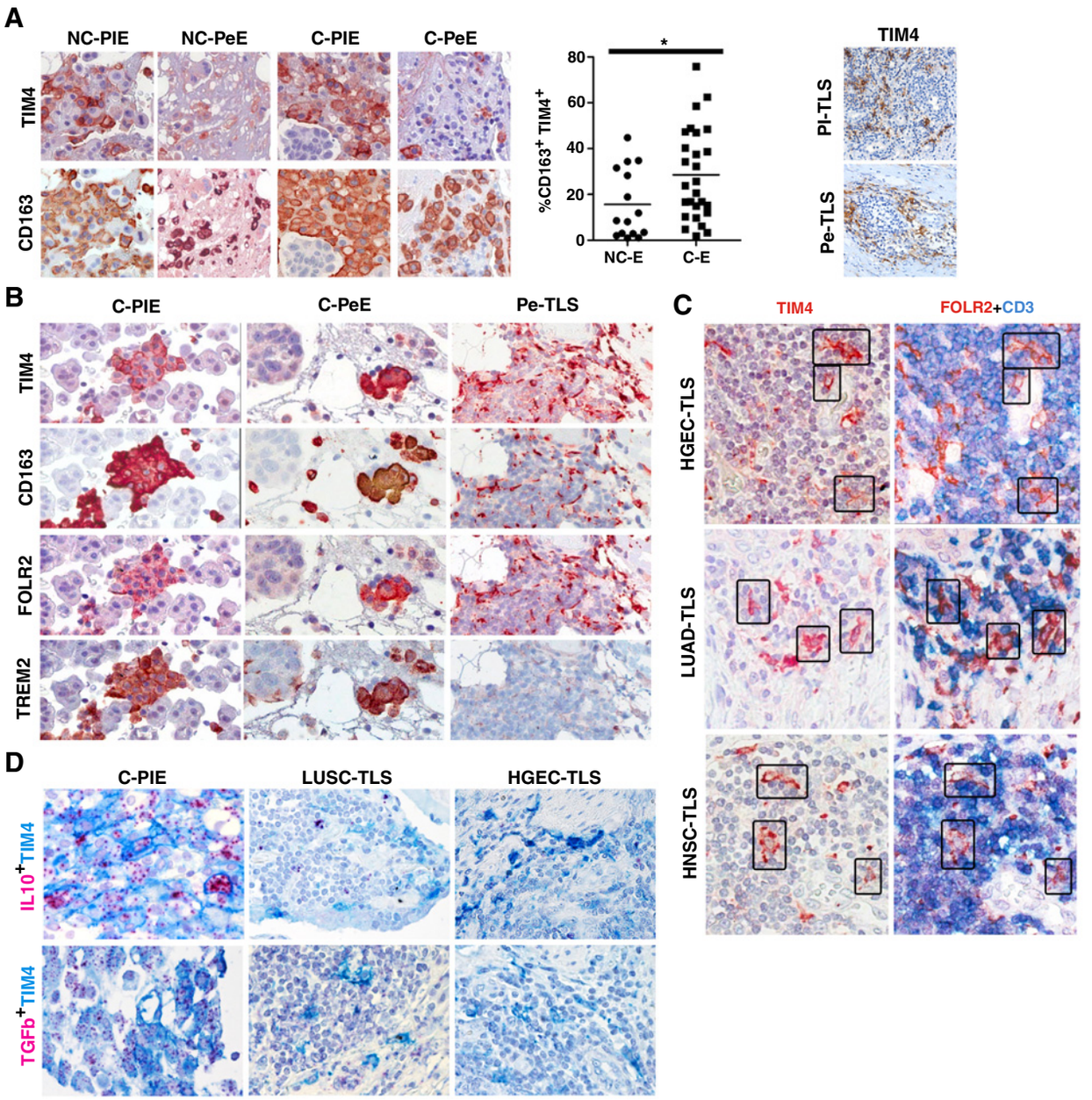

Figure 7.

Comparative phenotype of ^{CA}TIM4^{+} macrophages and ^{TLS}TIM4^{+} macrophages. Sections are from cell block obtained from human pleural (PIE) and peritoneal (PeE) effusion of noncancer (NC) and cancer (**C**) cases (**A, B, D**); pleural (PI-TLS) and peritoneal (Pe-TLS) biopsies containing TLS (**A** and **B**); a set of cancer containing TLS (**C** and **D**). TIM4^{+}macrophages represent a fraction of CD163^{+} macrophages in pleural and peritoneal effusion (**A**), with an increased percentage in cancer effusion compared with nonneoplastic fluid (graph in A); ^{TLS}TIM4^{+} macrophages are also identifiable in biopsies from pleural and peritoneal localization of carcinomas (**A**). Multiple sequential stains show ^{CA}TIM4^{+} macrophages strongly expressed FOLR2 and TREM2, whereas ^{TLS}TIM4^{+} macrophages lack TREM2 (**B**); ^{TLS}TIM4^{+}FOLR2^{+}TREM2^{-} macrophages interact with surrounding CD3^{+} T cells (**C**), as highlighted by a black rectangle. ^{CA}TIM4^{+} macrophages show abundant IL10 and TGFβ mRNA signals, whereas ^{TLS}TIM4^{+} macrophages are absent (**D**). Original **A–C** images are obtained from digital slides using 400× magnification; scale bar, 66 μm [sections from human pleural (PIE) and peritoneal (PeE) effusion in **A, B, C**], scale bar, 200 μm [sections from pleural (PI-TLS) and peritoneal (Pe-TLS) biopsies containing TLS in **A**]. Magnification 400× (**D**); scale bar, 50 μm. HGEC, high-grade endometrial carcinomas; LUAD, lung adenocarcinoma; HNSC, head and neck squamous cell carcinoma.

an alternative function of TIM4 in these cells. Based on their location and recurrent interaction with T cells (interfollicular and TLS T-cell zone), we propose their involvement in modulating T-cell responses.

The role of TIM4 in cancer immunity remains poorly explored. Based on this study, TIM4 is lacking in conventional tumor-infiltrating MΦ, whereas it marks cells in TLS, organized lymphoid structures found at the periphery of the tumor areas. $TIM4^+$ cells found in TLS express a set of MΦ-associated proteins, thus confirming their MΦ identity. Therefore, based on their localization, morphology, and phenotype, we propose that $^{TLS}TIM4^+M\Phi$ belong to a specific MΦ population distinct from classic tumor-infiltrating MΦ. $^{TLS}TIM4^+M\Phi$ in the T-cell compartment are poorly characterized. They might be involved in the regulation of antitumor effector responses developing in TLS. We observed that immunogenic cancers (including MSI^+ COAD, LUAD, and LUSC) are enriched in $TIM4^+M\Phi$-containing TLS, whose density directly correlates with the density of infiltrating $CD8^+$ T cells (this study and refs. 33 and 34). As previously reported (16), TLS represent privileged sites for local presentation of neighboring tumor antigens and subsequent activation of T- and B-cell responses. $^{TLS}TIM4^+M\Phi$ in the T-cell zone might thus instruct the antitumor adaptive immunity. $TIM4^+M\Phi$ coexpress FOLR2, characterized by members of our group as a marker of tissue-resident MΦ, located in the peritumoral stroma and associated with antitumor T-cell response (20). By exploring a pan-cancer scRNA-seq data set, we identified a cluster of cells coexpressing $TIM4^+FOLR2^+$ across human cancers. This cluster is enriched of MΦ-associated transcripts encoding for scavenger receptors, complement components, and MΦ chemokines. By subclustering of the same data set, we could identify two $TIM4^+FOLR2^+$ clusters. One cluster is enriched in markers of perivascular MΦ like *LYVE1*, *SLC40A1*, and *SEPP1* transcripts, whereas the other is reminiscent of immune-suppressive $TREM2^+$ MΦ (21,22). The function of *LYVE1*, *SLC40A1*, and *SEPP1* in macrophage biology is diverse and highlights the role of perivascular macrophages in regulating homeostatic and inflammatory processes (45–47). Among other DEG enriched in $^{TLS}TIM4^+M\Phi$, we also found genes associated with proinflammatory macrophages such as MT-CYB (48), MT-ATP6 (48), CTSB (49), and PLTP (50) or to some antitumor functions such as MAMDC2 (51). Finally, by survival analysis, a $^{TLS}TIM4^+M\Phi$ signature predicts a better OS and DFS.

By microscopic mapping of cell-block sections from pleural and peritoneal effusions of patients with carcinomas, we confirm the expression of TIM4 on cavitary MΦ. This $^{CA}TIM4^+M\Phi$ population is expanded in cancer patients (ovarian and lung carcinomas). Of note, $^{CA}TIM4^+M\Phi$ also express FOLR2; however, at variance with $^{TLS}TIM4^+M\Phi$, $^{CA}TIM4^+M\Phi$ express the immunosuppressive molecule TREM2 (21, 22), supporting their protumor phenotype, as revealed by studies in ovarian cancer (10, 14, 15). Notably, by exploring a pan-cancer data set, we could confirm that $^{CA}TIM4^+M\Phi$ signature predicts worse OS and DFS. TREM2 is induced in human monocytes and mouse bone marrow cells upon exposure to GM-CSF and CSF-1 (52, 53). We envisage that coexpression of TREM2 in $^{CA}TIM4^+M\Phi$ may reflect the abundance of these cytokines in the cavity fluid of cancer patients, as previously observed (54–56); alternatively, phenotypic and molecular differences between $^{TLS}TIM4^+M\Phi$ and $^{CA}TIM4^+M\Phi$ might result from a different origin of the two populations (resident vs. monocyte-derived). At variance with $^{TLS}TIM4^+M\Phi$, $^{CA}TIM4^+M\Phi$ expresses *IL10* and *TGFβ* mRNA, further supporting their immunosuppressive function. Accordingly, an increased frequency of Treg was observed in neoplastic cavitary fluids. These observations might suggest tailored intracavitary immunotherapy approaches for the effusion component of advanced cancers (57), as those targeting the immunosuppressive molecule TREM2 (38).

TIM4 is selectively expressed in resident macrophages across several tissues (58) including cavities and omental macrophages in cancer patients (10, 15). TIM4 expression is highly regulated by tissue-derived signals; however, the signals inducing its expression are not unequivocally characterized. Retinoic acid regulates gut-resident macrophages via GATA6 (59), whereas in mouse peritoneal macrophages, TIM4 is under the control of the transcription factors KLF2 and KLF4 (60). Further, the TIM4 promoter contains binding sites for STAT6 that regulate its expression via p300 (61). Data from our study suggest that two classes of TIM4-expressing macrophages with divergent functions exist in cancer tissues. It remains to be established whether $TIM4^+$ macrophages commonly acquire the marker and then further diversify in subtissue localization or coacquire TIM4 and divergent programs directly in the final tissue location.

In conclusion, the identification and localization of TIM4 expression on tumor-associated cells in human cancer have been severely limited by the lack of appropriate reagents (14). This study identifies for the first time a specific population of human MΦ, topographically distinct from conventional tumor-infiltrating MΦ, that localize in the T-cell zone of tumor-associated TLS. The exact role and clinical relevance of these cells in the antitumoral immune response require further research. $^{TLS}TIM4^+M\Phi$ are also found in immature nascent TLS; whether these cells can also play a role in lymphoid tissue induction is an unresolved question. A more extended characterization of these cells in comparison with other tumor-associated macrophages (including $TIM4^+$ germinal center macrophages in TLS) based on spatial "omics" approaches will further extend our knowledge on the heterogeneity of tumor-associated MΦ.

Authors' Disclosures

N. Caronni reports grants from AIRC during the conduct of the study. No disclosures were reported by the other authors.

Authors' Contributions

M. Bugatti: Data curation, formal analysis, investigation, methodology, writing–review and editing. **M. Bergamini:** Data curation, formal analysis, investigation, writing–original draft. **F. Missale:** Software, formal analysis, investigation, writing–review and editing. **M. Monti:** Data curation, methodology. **L. Ardighieri:** Resources, investigation. **I. Pezzali:** Formal analysis. **S. Picinoli:** Formal analysis. **N. Caronni:** Data curation, methodology. **Y. Missolo-Koussou:** Data curation, software, methodology, writing–original draft. **J. Helft:** Investigation, writing–original draft. **F. Benvenuti:** Conceptualization, investigation, writing–original draft, writing–review and editing. **W. Vermi:** Conceptualization, resources, supervision, funding acquisition, writing–original draft, writing–review and editing.

Acknowledgments

We would like to thank pathologists, technicians, clinicians, nurses, and administrative employers that have provided support to the study and to the follow-up of cancer patients. W. Vermi is funded by Associazione Italiana per la Ricerca sul Cancro (AIRC-IG-23179).

The publication costs of this article were defrayed in part by the payment of publication fees. Therefore, and solely to indicate this fact, this article is hereby marked "advertisement" in accordance with 18 USC section 1734.

Note

Supplementary data for this article are available at Cancer Immunology Research Online (http://cancerimmunolres.aacrjournals.org/).

Received April 8, 2022; revised June 24, 2022; accepted September 12, 2022; published first September 19, 2022.

References

1. Meyers JH, Chakravarti S, Schlesinger D, Illes Z, Waldner H, Umetsu SE, et al. TIM-4 is the ligand for TIM-1, and the TIM-1-TIM-4 interaction regulates T cell proliferation. Nat Immunol 2005;6:455–64.
2. Miyanishi M, Tada K, Koike M, Uchiyama Y, Kitamura T, Nagata S. Identification of Tim4 as a phosphatidylserine receptor. Nature 2007;450:435–9.
3. Kobayashi N, Karisola P, Peña-Cruz V, Dorfman DM, Jinushi M, Umetsu SE, et al. TIM-1 and TIM-4 glycoproteins bind phosphatidylserine and mediate uptake of apoptotic cells. Immunity 2007;27:927–40.
4. Rodriguez-Manzanet R, Sanjuan MA, Wu HY, Quintana FJ, Xiao S, Anderson AC, et al. T and B cell hyperactivity and autoimmunity associated with niche-specific defects in apoptotic body clearance in TIM-4-deficient mice. Proc Natl Acad Sci U S A 2010;107:8706–11.
5. Albacker LA, Yu S, Bedoret D, Lee W-L, Umetsu SE, Monahan S, et al. TIM-4, expressed by medullary macrophages, regulates respiratory tolerance by mediating phagocytosis of antigen-specific T cells. Mucosal Immunol 2013;6:580–90.
6. Shakhov AN, Rybtsov S, Tumanov AV, Shulenin S, Dean M, Kuprash DV, et al. SMUCKLER/TIM4 is a distinct member of TIM family expressed by stromal cells of secondary lymphoid tissues and associated with lymphotoxin signaling. Eur J Immunol 2004;34:494–503.
7. Dorfman DM, Hornick JL, Shahsafaei A, Freeman GJ. The phosphatidylserine receptors, T cell immunoglobulin mucin proteins 3 and 4, are markers of histiocytic sarcoma and other histiocytic and dendritic cell neoplasms. Hum Pathol 2010;41:1486–94.
8. Wong K, Valdez PA, Tan C, Yeh S, Hongo J-A, Ouyang W. Phosphatidylserine receptor Tim-4 is essential for the maintenance of the homeostatic state of resident peritoneal macrophages. Proc Natl Acad Sci U S A 2010;107:8712–7.
9. Zhang X, Liu Q, Wang J, Li G, Weiland M, Yu F-S, et al. TIM-4 is differentially expressed in the distinct subsets of dendritic cells in skin and skin-draining lymph nodes and controls skin Langerhans cell homeostasis. Oncotarget 2016;7:37498–512.
10. Etzerodt A, Moulin M, Doktor TK, Delfini M, Mossadegh-Keller N, Bajenoff M, et al. Tissue-resident macrophages in omentum promote metastatic spread of ovarian cancer. J Exp Med 2020;217.
11. Shaw TN, Houston SA, Wemyss K, Bridgeman HM, Barbera TA, Zangerle-Murray T, et al. Tissue-resident macrophages in the intestine are long lived and defined by Tim-4 and CD4 expression. J Exp Med 2018;215:1507–18.
12. Baghdadi M, Yoneda A, Yamashina T, Nagao H, Komohara Y, Nagai S, et al. TIM-4 glycoprotein-mediated degradation of dying tumor cells by autophagy leads to reduced antigen presentation and increased immune tolerance. Immunity 2013;39:1070–81.
13. Caronni N, Piperno GM, Simoncello F, Romano O, Vodret S, Yanagihashi Y, et al. TIM4 expression by dendritic cells mediates uptake of tumor-associated antigens and anti-tumor responses. Nat Commun 2021;12.
14. Xia H, Li S, Li X, Wang W, Bian Y, Wei S, et al. Autophagic adaptation to oxidative stress alters peritoneal residential macrophage survival and ovarian cancer metastasis. JCI insight 2020;5:e141115.
15. Chow A, Schad S, Green MD, Hellmann MD, Allaj V, Ceglia N, et al. Tim-4(+) cavity-resident macrophages impair anti-tumor CD8(+) T cell immunity. Cancer Cell 2021;39:973–88.e9.
16. Sautès-Fridman C, Petitprez F, Calderaro J, Fridman WH. Tertiary lymphoid structures in the era of cancer immunotherapy. Nat Rev Cancer 2019;19:307–25.
17. Nerviani A, Pitzalis C. Role of chemokines in ectopic lymphoid structures formation in autoimmunity and cancer. J Leukoc Biol 2018;104:333–41.
18. Helmink BA, Reddy SM, Gao J, Zhang S, Basar R, Thakur R, et al. B cells and tertiary lymphoid structures promote immunotherapy response. Nature 2020;577:549–55.
19. Cabrita R, Lauss M, Sanna A, Donia M, Skaarup Larsen M, Mitra S, et al. Tertiary lymphoid structures improve immunotherapy and survival in melanoma. Nature 2020;577:561–5.
20. Nalio Ramos R, Missolo-Koussou Y, Gerber-Ferder Y, Bromley CP, Bugatti M, Núñez NG, et al. Tissue-resident FOLR2(+) macrophages associate with CD8(+) T cell infiltration in human breast cancer. Cell 2022;185:1189–207.
21. Molgora M, Esaulova E, Vermi W, Hou J, Chen Y, Luo J, et al. TREM2 modulation remodels the tumor myeloid landscape enhancing anti-PD-1 immunotherapy. Cell 2020;182:886–900.
22. Katzenelenbogen Y, Sheban F, Yalin A, Yofe I, Svetlichnyy D, Jaitin DA, et al. Coupled scRNA-seq and intracellular protein activity reveal an immunosuppressive role of TREM2 in cancer. Cell 2020;182:872–85.
23. Vermi W, Micheletti A, Lonardi S, Costantini C, Calzetti F, Nascimbeni R, et al. slanDCs selectively accumulate in carcinoma-draining lymph nodes and marginate metastatic cells. Nat Commun 2014;5:3029.
24. Coppola D, Nebozhyn M, Khalil F, Dai H, Yeatman T, Loboda A, et al. Unique ectopic lymph node-like structures present in human primary colorectal carcinoma are identified by immune gene array profiling. Am J Pathol 2011;179:37–45.
25. Calderaro J, Petitprez F, Becht E, Laurent A, Hirsch TZ, Rousseau B, et al. Intratumoral tertiary lymphoid structures are associated with a low risk of early recurrence of hepatocellular carcinoma. J Hepatol 2019;70:58–65.
26. Van der Maaten L, Hinton G. Visualizing data using t-SNE. J Mach Learn Res 2008;9.
27. Azizi E, Carr AJ, Plitas G, Cornish AE, Konopacki C, Prabhakaran S, et al. Single-cell map of diverse immune phenotypes in the breast tumor microenvironment. Cell 2018;174:1293–308.
28. Geissmann F, Dieu-Nosjean MC, Dezutter C, Valladeau J, Kayal S, Leborgne M, et al. Accumulation of immature Langerhans cells in human lymph nodes draining chronically inflamed skin. J Exp Med 2002;196:417–30.
29. Mantovani A, Marchesi F, Jaillon S, Garlanda C, Allavena P. Tumor-associated myeloid cells: diversity and therapeutic targeting. Cell Mol Immunol 2021;18:566–78.
30. Lopez-Yrigoyen M, Cassetta L, Pollard JW. Macrophage targeting in cancer. Ann N Y Acad Sci 2021;1499:18–41.
31. Mulder K, Patel AA, Kong WT, Piot C, Halitzki E, Dunsmore G, et al. Cross-tissue single-cell landscape of human monocytes and macrophages in health and disease. Immunity 2021;54:1883–900.
32. Mattiola I, Tomay F, De Pizzol M, Silva-Gomes R, Savino B, Gulic T, et al. The macrophage tetraspan MS4A4A enhances dectin-1-dependent NK cell–mediated resistance to metastasis. Nat Immunol 2019;20:1012–22.
33. Loupakis F, Depetris I, Biason P, Intini R, Prete AA, Leone F, et al. Prediction of benefit from checkpoint inhibitors in mismatch repair deficient metastatic colorectal cancer: role of tumor infiltrating lymphocytes. Oncologist 2020;25:481–7.
34. Lin A, Zhang J, Luo P. Crosstalk between the MSI status and tumor microenvironment in colorectal cancer. Front Immunol 2020;11:2039.
35. De' Angelis GL, Bottarelli L, Azzoni C, De' Angelis N, Leandro G, Di Mario F, et al. Microsatellite instability in colorectal cancer. Acta Biomed 2018;89:97–101.
36. Qian J, Olbrecht S, Boeckx B, Vos H, Laoui D, Etlioglu E, et al. A pan-cancer blueprint of the heterogeneous tumor microenvironment revealed by single-cell profiling. Cell Res 2020;30:745–62.
37. Ardighieri L, Missale F, Bugatti M, Gatta LB, Pezzali I, Monti M, et al. Infiltration by CXCL10 secreting macrophages is associated with antitumor immunity and response to therapy in ovarian cancer subtypes. Front Immunol 2021;12:690201.
38. Binnewies M, Pollack JL, Rudolph J, Dash S, Abushawish M, Lee T, et al. Targeting TREM2 on tumor-associated macrophages enhances immunotherapy. Cell Rep 2021;37:109844.
39. Gray EE, Cyster JG. Lymph node macrophages. J Innate Immun 2012;4:424–36.
40. Wakimoto T, Tomisaka R, Nishikawa Y, Sato H, Yoshino T, Takahashi K. Identification and characterization of human thymic cortical dendritic macrophages that may act as professional scavengers of apoptotic thymocytes. Immunobiology 2008;213:837–47.
41. Paessens LC, Fluitsma DM, van Kooyk Y. Haematopoietic antigen-presenting cells in the human thymic cortex: evidence for a role in selection and removal of apoptotic thymocytes. J Pathol 2008;214:96–103.
42. Yeo JH, Lam YW, Fraser ST. Cellular dynamics of mammalian red blood cell production in the erythroblastic island niche. Biophys Rev 2019;11:873–94.
43. Fraser ST, Midwinter RG, Coupland LA, Kong S, Berger BS, Yeo JH, et al. Heme oxygenase-1 deficiency alters erythroblastic island formation, steady-state erythropoiesis and red blood cell lifespan in mice. Haematologica 2015;100:601–10.
44. Vermi W, Micheletti A, Finotti G, Tecchio C, Calzetti F, Costa S, et al. Slan+ monocytes and macrophages mediate CD20-dependent b-cell lymphoma elimination via ADCC and ADCP. Cancer Res 2018;78:3544–59.
45. Chakarov S, Lim HY, Tan L, Lim SY, See P, Lum J, et al. Two distinct interstitial macrophage populations coexist across tissues in specific subtissular niches. Science 2019;363:eaau0964.
46. Knutson MD, Oukka M, Koss LM, Aydemir F, Wessling-Resnick M. Iron release from macrophages after erythrophagocytosis is up-regulated by ferroportin 1 overexpression and down-regulated by hepcidin. Proc Natl Acad Sci U S A 2005;102:1324–8.

47. Kaushal N, Kudva AK, Patterson AD, Chiaro C, Kennett MJ, Desai D, et al. Crucial role of macrophage selenoproteins in experimental colitis. J Immunol 2014;193:3683–92.
48. Takiguchi H, Yang CX, Yang CWT, Sahin B, Whalen BA, Milne S, et al. Macrophages with reduced expressions of classical M1 and M2 surface markers in human bronchoalveolar lavage fluid exhibit pro-inflammatory gene signatures. Sci Rep 2021;11:8282.
49. Sendler M, Weiss F-U, Golchert J, Homuth G, van den Brandt C, Mahajan UM, et al. Cathepsin B-mediated activation of trypsinogen in endocytosing macrophages increases severity of pancreatitis in mice. Gastroenterology 2018;154:704–18.
50. Desrumaux C, Lemaire-Ewing S, Ogier N, Yessoufou A, Hammann A, Sequeira-Le Grand A, et al. Plasma phospholipid transfer protein (PLTP) modulates adaptive immune functions through alternation of T helper cell polarization. Cell Mol Immunol 2016;13:795–804.
51. Lee H, Park B-C, Soon Kang J, Cheon Y, Lee S., Jae Maeng P. MAM domain containing 2 is a potential breast cancer biomarker that exhibits tumour-suppressive activity. Cell Prolif 2020;53:e12883.
52. Bouchon A, Hernández-Munain C, Cella M, Colonna M. A DAP12-mediated pathway regulates expression of CC chemokine receptor 7 and maturation of human dendritic cells. J Exp Med 2001;194:1111–22.
53. Turnbull IR, Gilfillan S, Cella M, Aoshi T, Miller M, Piccio L, et al. Cutting edge: TREM-2 attenuates macrophage activation. J Immunol 2006;177:3520–4.
54. Blondy T, d'Almeida SM, Briolay T, Tabiasco J, Meiller C, Chéné A-L, et al. Involvement of the M-CSF/IL-34/CSF-1R pathway in malignant pleural mesothelioma. J Immunother cancer 2020;8:e000182.
55. Chechlinska M, Kaminska J, Markowska J, Kramar A, Steffen J. Peritoneal fluid cytokines and the differential diagnosis of benign and malignant ovarian tumors and residual/recurrent disease examination. Int J Biol Markers 2007;22:172–80.
56. Punnonen R, Teisala K, Kuoppala T, Bennett B, Punnonen J. Cytokine production profiles in the peritoneal fluids of patients with malignant or benign gynecologic tumors. Cancer 1998;83:788–96.
57. Donnenberg VS, Wagner PL, Luketich JD, Bartlett DL, Donnenberg AD. Localized intra-cavitary therapy to drive systemic anti-tumor immunity. Front Immunol 2022;13:846235.
58. Blériot C, Chakarov S, Ginhoux F. Determinants of resident tissue macrophage identity and function. Immunity 2020;52:957–70.
59. Okabe Y, Medzhitov R. Tissue-specific signals control reversible program of localization and functional polarization of macrophages. Cell 2014;157:832–44.
60. Roberts AW, Lee BL, Deguine J, John S, Shlomchik MJ, Barton GM. Tissue-resident macrophages are locally programmed for silent clearance of apoptotic cells. Immunity 2017;47:913–27.
61. Yang B, Li L-J, Xu L-Z, Liu J-Q, Zhang H-P, Geng X-R, et al. Histone acetyltransferease p300 modulates TIM4 expression in dendritic cells. Sci Rep 2016;6:21336.